GEOPHYSICS. VOL. 76, NO. 6 (NOVEMBER-DECEMBER 2011); P. WC159–WC168, 9 FIGS., 1 TABLE.
10.1190/GEO2011-0057.1

Inferring rock fracture evolution during reservoir stimulation from seismic anisotropy

Andreas Wuestefeld[1], James P. Verdon[2], J-Michael Kendall[2], James Rutledge[3], Huw Clarke[4], and James Wookey[2]

ABSTRACT

We have analyzed seismic anisotropy using shear-wave-splitting measurements made on microseismic events recorded during a hydraulic fracture experiment in a tight gas reservoir in Carthage, east Texas. Microseismic events were recorded on two downhole arrays of three-component sensors, the geometry of which provided good ray coverage for anisotropy analysis. A total of 16,633 seismograms from 888 located events yielded 1545 well-constrained shear-wave-splitting measurements. Manual analysis of splitting from a subset of this data set reveals temporal changes in splitting during fracturing. Inversion using the full data set allows the identification of fracture strike and density, which is observed to vary during fracturing. The recovered fracture strike in the rock mass is parallel to directions of regional borehole breakout, but oblique to the hydraulic fracture corridor as mapped by the microseismic event. We relate this to en-echelon fracturing of preexisting cracks. The magnitude of shear-wave splitting shows a clear temporal increase during each pumping stage, indicating the generation of cracks and fissures in a halo around the fracture corridor, which thus increase the overall permeability of the rock mass. Our results show that shear-wave-splitting analysis can provide a useful tool for monitoring spatial and temporal variations in fracture networks generated by hydraulic stimulation.

INTRODUCTION

Seismic studies of rock fractures provide valuable insights into the state of stress and are useful in a number of applications. In geotechnical and mining environments, knowledge of fracture orientation can be important in hazard assessment, but may also help guide excavation programs. In reservoirs, fractures provide important secondary porosity and permeability, which may or may not be desirable. To prevent unwanted leakage, subsurface CO_2 storage projects require that injection does not stimulate fracturing in the sealing overburden (e.g., Verdon et al., 2009). In geothermal projects, fractures increase not only permeability, but also the effective contact surface, which facilitates the heat transport from rock to the transfer fluid.

Reservoir formations may contain large quantities of oil or gas, but have a poor flow rate due to low permeability. This is particularly true for tight sands, shale gas, and coalbed methane. Cracks, or natural fractures, exist in most of these reservoirs, but they often lack connectivity. Hydraulic stimulation can be used to generate fracture networks and to improve the permeability. The resulting fractures and cracks will tend to align with direction of dominant horizontal stress, thus generating a permeability anisotropy.

A medium with aligned fractures can be approximated as an effectively homogeneous but anisotropic medium, if the dominant seismic wavelength is much longer than the fracture spacing and size (e.g., Kachanov, 1980; Crampin, 1984; Hall and Kendall, 2003). For a single set of vertical aligned fractures in an isotropic medium, this results in hexagonal symmetry with a horizontal axis

Manuscript received by the Editor 9 February 2011; revised manuscript received 8 August 2011; published online 30 December 2011.
[1]Formerly University of Bristol, Department of Earth Sciences, Bristol, U.K.; presently ESG Solutions, Kingston, Ontario, Canada. E-mail: andreas.wuestefeld@esg.ca.
[2]University of Bristol, Department of Earth Sciences, Bristol, U.K. Canada. E-mail: James.Verdon@bristol.ac.uk; gljmk@bristol.ac.uk; j.wookey@bristol.ac.uk.
[3]Los Alamos National Laboratories, Geophysics Group, Los Alamos, New Mexico, USA. E-mail: jrutledge@lanl.gov.
[4]Formerly University of Bristol, Department of Earth Sciences, Bristol, U.K.; presently Cuadrilla Resources Ltd., Lichfield, U.K. E-mail: huw.clarke@cuadrillaresources.com.

of symmetry (horizontal transverse isotropy (HTI). However, other factors can also generate anisotropy. These include the alignment of grain-scale microcracks (Hall et al., 2008), which can be modulated by nonhydrostatic stress changes (Zatsepin and Crampin, 1997; Verdon et al., 2008), the periodic thin layering of contrasting lithologies (Backus, 1964), and the preferred alignment of intrinsically anisotropic crystals (Raymer et al., 2000; Valcke et al., 2006). In sedimentary rocks, these mechanisms can be also very effective in generating anisotropy with a hexagonal symmetry, but in general with a vertical axis of symmetry (vertical transverse isotropy, VTI). In reality both mechanisms will be at play in sedimentary basins, which render the bulk rock anisotropic, but with an orthorhombic symmetry. Furthermore, structural deformation and stress anisotropy can lead to even more degenerate forms of anisotropy (e.g., monoclinic and triclinic symmetry).

A seismic shear wave entering an anisotropic medium will, in general, split into two independent, orthogonally polarized S-waves. The polarizations of the fast and slow shear waves and the separation in the arrival time of each of them can be used to characterize the magnitude and symmetry of the anisotropy. The delay time between the two waves is proportional to the strength of S-wave velocity anisotropy and the length of the raypath within the anisotropic medium. Wuestefeld et al. (2010) recently developed a workflow for the automated measurement of these shear-wave-splitting parameters with large data sets.

The splitting parameters will vary with ray direction, in a way that is characteristic of the anisotropy system, and hence, the underlying cause of the anisotropy. For example, shear-wave splitting can be used to characterize aligned fracture sets (Crampin, 1984; Kendall et al., 2005; Keir et al., 2005; Al-Harrasi et al., 2011a) and to study the temporal evolution of fractures (Gerst and Savage, 2004; Wuestefeld et al., 2011). Furthermore, the frequency-dependent nature of fracture-induced anisotropy can be used to estimate dominant fracture size (Al-Harrasi et al., 2011b). More generally, Verdon et al. (2009) introduced a method for inverting splitting parameters for fracture strike and density, which also accounts for the presence of shear-wave anisotropy induced by the intrinsic sedimentary fabric of the rock.

It is worth noting that more traditional passive seismic methods, such as those for estimating event locations and source mechanisms, give information about the source region, whereas shear-wave splitting is a raypath effect and thus provides valuable information about the surrounding rock mass. Used in conjunction with such other microseismic analysis techniques, shear-wave splitting can be used to help calibrate geomechanical and fluid-flow models of reservoirs (e.g., Angus et al., 2010).

Here, we study shear-wave splitting during hydraulic fracture stimulation in a gas field within the Cotton Valley formation in Carthage, East Texas (Walker, 1997; Rutledge et al., 2004). Hydraulic fracturing is a common technique used to enhance the production of oil and natural gas by stimulating fractures that extend from the wellbore into the surrounding rock. Typically, fluids injected underground at high pressures fracture the formation, and the oil or gas flows more freely out of the rock matrix. Usually, a "proppant" is suspended in the fluid to keep the fracture open (e.g., Jones and Britt, 2009). Monitoring microseismic activity helps better understand the response of the rock to changing stress conditions and map the fracture. In turn, mapping the microseismicity indicates the fracture network complexity and might thus help understand and improve proppant emplacement. We investigate what further insights into fracturing in the rock mass can be obtained from shear-wave-splitting studies.

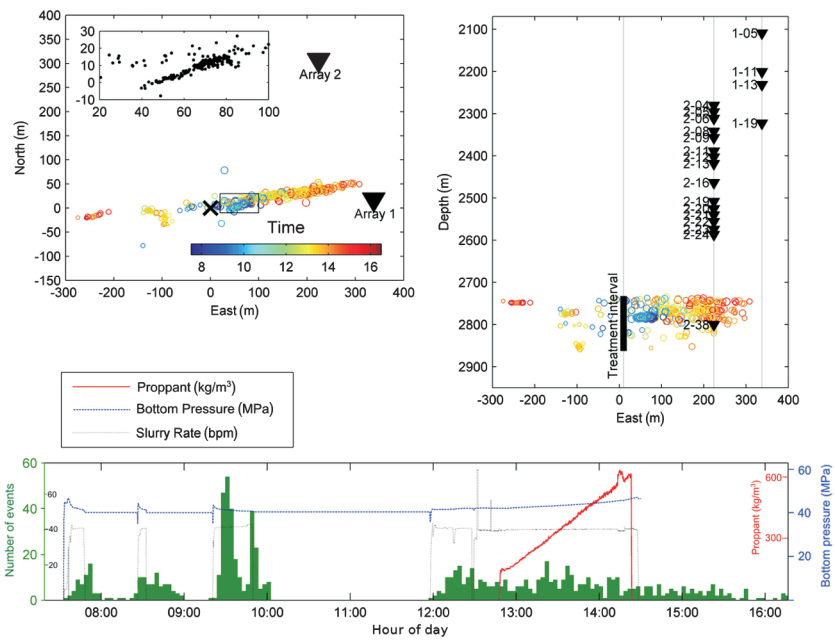

Figure 1. Events and receiver locations of the Cotton Valley data set in map-view (top-left) with inset showing details of the cluster region marked within a box, and in cross-section (top-right). Color indicates timing of the events during stimulation (see legend in upper left panel — time is in hours). A fracture corridor develops oriented at N80°E. A secondary fracture (see inset) opens oriented N65°E between 30 and 75 m east of the injection well (marked as a black cross). The lower panel shows a histogram of seismicity in 3 minute bins (green), the variation of pumping pressure (blue), slurry rate (black), and cumulative proppant density injected during stimulation (red).

The Cotton Valley data set

The Cotton Valley formation consists of silicastic sandstones with intermittent shale and carbonate horizons over a total thickness of approximately 325 m (Rutledge and Phillips, 2003). The reservoir is typical of low-permeability gas resources that require hydraulic fracture stimulation for economic production. The current understanding of the fracture process assumes that tensile opening dominates at the fracture tip, while shear failure occurs simultaneously along the entire fault length (e.g., Rutledge et al., 2004). In another deep hydraulic fracturing experiment, Ake et al. (2005) found that 89% of the events were strike-slip, while the remaining events where roughly equally divided between normal and thrust faulting events. More recent studies found evidence for a nondouble-couple component in event mechanisms associated with hydraulic fracturing (Foulger et al., 2004; Šílený et al, 2009).

We focus on microseismic events from a gel frac-job at the base of the Upper Cotton Valley formation, named "Treatment B" in Rutledge et al. (2004). The events generally occur in

discrete, thin bands, which correlate with the perforation intervals targeted for fracturing (Figure 1). The events occur along a general trend of N83ºE. Furthermore, Rutledge et al. (2004)note that an anomalously high event count is found within small clusters. Especially, one cluster contains 42% of the events and develops at a shallow angle from the general trend at N65°E. This structure develops westward, toward the injection well (Figure 1). Rutledge et al. (2004) associate this cluster with a preexisting fault that has been reactivated by the back stream of fluid.

RESULTS

We performed manual shear-wave-splitting analysis (Table 1) on the waveforms of station 1–11 (Figure 1) using a version of the processing software SplitLab (Wuestefeld et al., 2008), adapted for reservoir studies. Station 1–11, located close to the top of Array 1, recorded a large number of good quality seismograms with clear S-wave arrivals. Relatively steep raypaths make events recorded at this station strongly susceptible to shear-wave anisotropy caused by vertical fractures (e.g., Verdon et al., 2009). The mean take-off angle from vertical toward the station is 30°. In general, any anisotropy generated by vertical fractures is best sensed with sensors from the top part of the array, whereas sensors near the bottom of the array will be more sensitive to anisotropy due to the sedimentary fabric (Verdon et al., 2009; Wuestefeld et al., 2010).

The focus here was on events from within the localized cluster of events during the third pressure stage (Figure 1). The anisotropy is smallest for events early in the development of fracturing and increases in time. The increase of anisotropy with time is clearly shown in Figure 2a. However, the event locations also propagate westward during this time (Figure 2b), and the increase may be explained by spatial variations in anisotropy. This entanglement of spatial and temporal variation is inherent to many production related studies: is the increase in observed change due to heterogeneity, or is it due to temporal changes caused by continuous fracking? In the following, we address this issue by considering differences in the raypaths.

Our manual analysis of shear-wave splitting at station 1–11 (Table 1) shows an increase in delay time within a 30-minute period from 3 to 7.25 ms for events within 26 m of each other. This change cannot be explained by changes in raypath length (see Figure 2c): The maximum hypocentral distance between the events is 26 m, resulting in a maximum path length difference with station 1–11 of 15.05 m. As the raypaths are nearly identical, the increase in delay time from 3 to 7.25 ms would need to be accrued in this extra 15 m. Quantitatively, this would require 84% shear-wave anisotropy in this small isolated region (assuming a velocity of 3000 m/s, which is the mean S-wave velocity at the depth of the Cotton Valley event). Because this is unrealistically high, we conclude that the observed change in shear-wave splitting delay time is indeed a temporal effect.

This temporal increase can be explained by an increase in crack density in the subsurface due to fluid injection. This volume increase reactivates natural cracks and fissures of favorable orientation due to stress transfer (e.g., Rozhko, 2010; Schoenball et al., 2010). The alignment of the reactivated cracks will thus increase the anisotropy within a "halo" around the hydraulic fracture. If we allow for a shear-wave-velocity anisotropy of between 10% and 15% caused by aligned cracks, this suggests ($\Delta s = V_{S_{mean}} \times 100 \times \Delta dt/A$) a halo radius between 127.5 and 85 m, respectively. The region affected by stress changes due to fluid injection can thus be narrowed to this radius around the observed seismicity. Note that the halo is not symmetric and this length is not necessarily

Table 1. Parameters and shear-wave splitting results of the events used in the manual analysis of records at station 1–11. Note the increase in delay time over time at similar source-receiver distances. Event locations and magnitudes are from Rutledge et al. (2004). The errors in delay time, dterr, are calculated using an f-test as described in Silver and Chan (1991).

Time	Lat (m)	Long (m)]	Depth (m)	Distance (m)	Event Magnitude (Mw)	Splitting delay time (ms)	Delay time error (ms)	Percent anisotropy	Percent anisotropy error
09:24:41	11.55	71.04	2780.73	638.60	−1.80	3.000	0.375	1.41	0.18
09:28:45	12.39	71.73	2781.16	638.68	−1.76	3.500	0.250	1.64	0.12
09:29:05	10.60	68.49	2780.59	639.55	−1.66	4.500	0.188	2.11	0.09
09:31:55	10.61	69.52	2780.41	638.95	−1.65	4.250	0.125	2.00	0.06
09:33:04	10.56	69.73	2780.59	639.03	−1.70	4.250	0.313	2.00	0.15
09:37:24	10.82	69.25	2780.30	638.96	−1.45	4.750	0.313	2.23	0.15
09:48:24	2.22	51.04	2783.23	649.63	−1.79	6.250	0.438	2.89	0.20
09:48:48	8.99	66.93	2780.31	639.97	−1.80	5.250	0.625	2.46	0.29
09:49:48	4.01	59.15	2785.22	647.83	−1.76	7.000	0.313	3.24	0.14
09:49:54	3.34	53.61	2783.21	648.46	−1.74	6.000	0.250	2.78	0.12
09:50:23	3.83	58.61	2785.42	648.25	−1.79	7.500	0.250	3.47	0.12
09:51:05	3.31	53.90	2783.50	648.59	−1.74	6.250	0.313	2.89	0.14
09:54:37	0.02	48.44	2786.37	653.65	−1.74	7.250	0.250	3.33	0.11
09:56:11	2.70	53.40	2780.87	646.46	−1.73	6.500	0.250	3.02	0.12

the radius of a sphere, but rather that of an ellipsoid oriented between events and station.

Full data set processing and inversion

Increasingly large data sets make manual shear-wave-splitting processing impractical. Automatic processing improves the objectivity and repeatability of measurements. Here, we use the automated shear-wave splitting technique presented by Wuestefeld et al. (2010), which is based on characteristic differences in two independent splitting inversion techniques (Wuestefeld and Bokelmann, 2007) and multiwindow analysis (Teanby et al., 2004). The automated analysis returns a quality index, which can vary from −1.0 for null to 0.0 for poor to +1.0 for good splitting measurements (see Wuestefeld et al., 2010).

For the Cotton Valley data set we extend the analysis to the entire period of monitoring. Rutledge et al. (2004) report 888 located events for this treatment. The data set thus consists of 16,633 source-receiver records of which 1545 resulted in good splitting measurements. Good splitting measurements are defined here as having a quality index of above 0.85, a signal-to-noise of $S/R > 4$, delay times between $0.5 \leq dt \leq 9$ ms, an error in delay time smaller than 2 ms and an error in fast-polarization directions smaller than 15°.

Figure 3 shows the resulting delay times from automation for all stations during the third stimulation phase. Note the equivalent increase in delay time for station 1–11 presented in Figure 2a. Overall, the shallower stations (cf. Figure 1), with steep incidence angles, show significant variations in delay time during this stimulation. Shallower stations exhibit only minimal variations, albeit with a higher starting level. The fast polarization directions for the entire data set are shown in Figure 4. Steep incident rays show fast polarizations subparallel to the ray direction, whereas shallower incident waves result in ray-perpendicular fast-polarization directions.

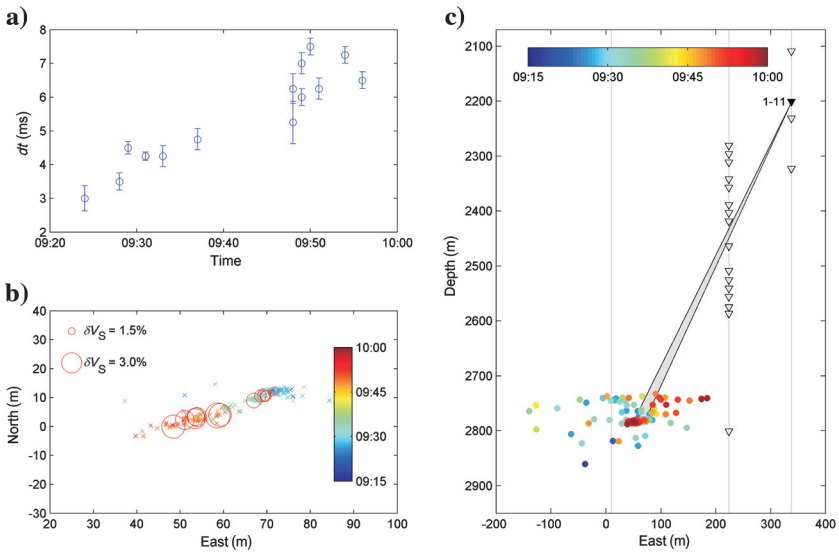

Figure 2. Observed splitting delay time at station 1–11 during the third pumping stage (cf. Figure 1, bottom). Note that delay time increase can be attributed to either temporal (a) or spatial (b) change in anisotropy. (c) Cross section of the (straight line) travel paths. Rays from either end of the reactivated fracture essentially travel the same path and map the same Fresnel zones. Thus, when excluding temporal effects, any difference in delay time would have to be accumulated by an unrealistically strong anisotropy heterogeneity between the two event locations.

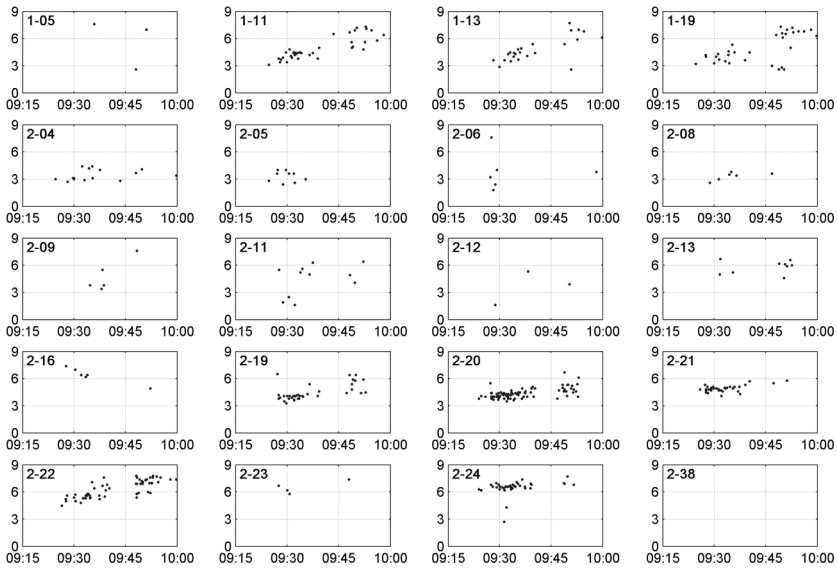

Figure 3. Delay time (in milliseconds) at all stations of the array during the third pumping stage, as calculated using automatic processing. The station label is in the top left corner of each panel. Note that deeper stations observe a smaller increase in delay time, but start at a higher background level. This is attributed to the fact that shallow incident waves are more sensitive to the intrinsic anisotropy of the host rock and steep incident waves are more sensitive to the anisotropy induced by vertical fractures.

To understand these variations in delay times and fast polarization directions between stations in terms of changes in fracture strike (α) and density (ξ), we invert our observations for fracture parameters using a rock-physics-based approach based on Verdon et al. (2009). For a similar approach to invert for the entire set of orthorhombic parameters, using P- and S-waves, see Tsvankin (1997), Grechka et al. (1999) and Bakulin et al. (2000). Our model assumes that the observed shear-wave splitting is caused by aligned vertical fractures set in a rock with VTI symmetry described by Thomsen's (1986) ε, γ, and δ parameters. Although such an approach can be generalized to allow for dipping cracks or multiple crack sets (e.g., Verdon et al., 2011), attempts to invert for two fracture sets with the Cotton Valley data set suggest that a single fracture set is most appropriate.

Initially, we invert the full data set of shear-wave-splitting measurements, using fixed values for V_P and V_S based on the velocity model used during event location, with ε, γ, δ, α, and ξ as free parameters. The results are plotted in Figure 5. Figure 5a shows the shear-wave-splitting observations overlain on the best fitting rock-physics model. Figure 5b and 5k shows slices of the misfit hypercube between rock-physics model and observation. The inversion recovers the following values: fracture strike $(\alpha) =$ N66E(± 3), fracture density $(\xi) = 0.024(\pm 0.002)$, and $\gamma = 0.12(\pm 0.01)$. Examining the misfit hypercube reveals a trade-off between ε and δ (Figure 5j), implying that neither is well-constrained. Further discussion on the ability of the inversion process to accurately recover the free parameters is included in Appendix A. The trade-off between ε and δ allows us to remove ε from the free parameters that we invert for, instead arbitrarily fixing it to $\varepsilon = 2\gamma$, so long as we accept that δ is poorly constrained. This significantly improves the computational expense of our grid-search based inversion procedure, and so we follow this for our analysis of temporal variations below.

The inversion result of γ of $0.12(\pm 0.01)$ is comparable, but not equal to, the value of $\gamma = 0.18$ measured by Thomsen (1986) for a laboratory sample of Cotton Valley shale. We note here the difficulties in comparing isolated rock samples measured in the laboratory, whereas our values are based on in situ measurements through the whole rock mass, and are thus arguably more representative for uses in other seismic or modeling methods.

The inversion images fractures striking at N66°E. The borehole breakout orientations given in the World Stress Map (Heidbach et al., 2008) rotate from north-northeast to south-southwest in southern Texas to east-northeast to west-southwest in the Cotton Valley area (Figure 6). Interestingly, two borehole breakout measurements in that area from a hydraulic fracture experiments deviate slightly from this general trend. In northwest Louisiana, Strubhar et al. (1975) report a borehole breakout orientation of N90°E, comparable to the N83°E hydraulic fracture trend observed in Cotton Valley. In a study of cores mainly from the Travis Peak formation, which overlies the Cotton Valley formation, Laubach (1988) found two distinct fracture trends: one set of natural and coring induced cracks with a mean strike of N83°E, and a second set of natural cracks that strikes between N65°E and N74°E. The crack strike of our inversion is oblique to the strike of the hydraulic fracture as mapped by the microseismic events (N83°E, Figure 1), but it agrees well with the orientation of that second natural crack set and also with the general regional trend in east Texas as seen in borehole break outs (Figure 6). This indicates that stress change may reactivate mostly the cracks of orientation N65°E, as seen by shear-wave splitting, and the hydraulic fracture develops oblique to these cracks in an en-echelon style.

We next analyzed temporal changes observed in the whole data set, similar to Figure 2, where we described the increase in delay time and thus magnitude of anisotropy during the third pumping stage. We attributed this to the development and reactivation of cracks and fissures in the surrounding rock. This hypothesis can be tested by applying the above inversion technique to results from sliding time windows. Such an approach has been successfully applied to an underground mining data set to monitor fracture evolution during a production cycle (Wuestefeld et al., 2011). We chose a 30-minute time window of events from the cluster region and calculated the inversion parameters in time steps of 6 minutes. We only used windows with more than 10 measurements. In these inversions, ε is fixed, γ, δ, α and ξ are free parameters. Our error analysis in Appendix A suggests that such an approach will allow α, ξ and γ to be constrained, leaving δ unresolved. Figure 7 shows the resulting evolution of fracture density and strike found by the inversion. Interestingly, crack density increases during each injection phase, but returns to a lower level. There are also minor decreases in crack density at around 12:30 and 13:00. The increase in crack density is most prominent after pumping stopped. Our preferred interpretation is that the additional crack density caused by injection is offset by compression of the surrounding rock and thus crack closure. Immediately after "shut-in," the rock begins to relax

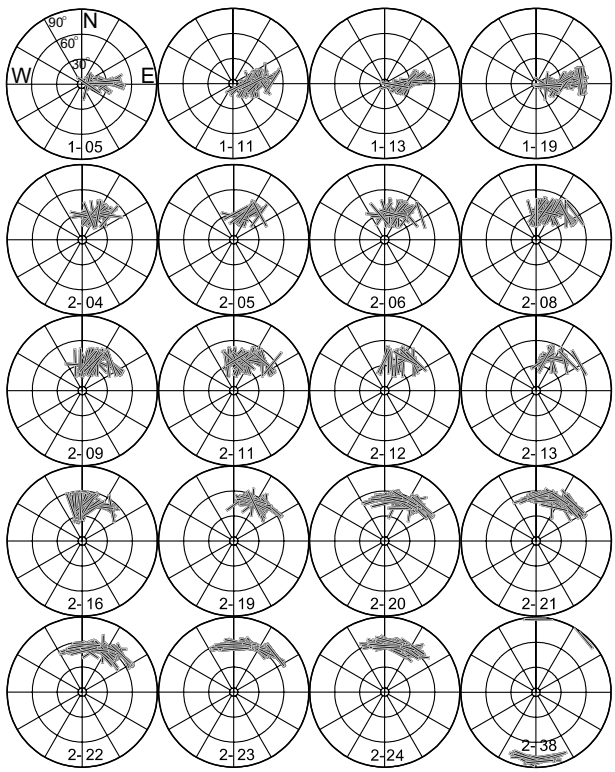

Figure 4. Upper hemisphere plots of fast S-wave polarization directions for the different stations for the whole treatment. Observed fast shear-wave orientations at each station are plotted at their respective azimuth and take-off angle, where vertical raypath plot in the center and horizontal raypaths plot on the outer rim of each hemisphere.

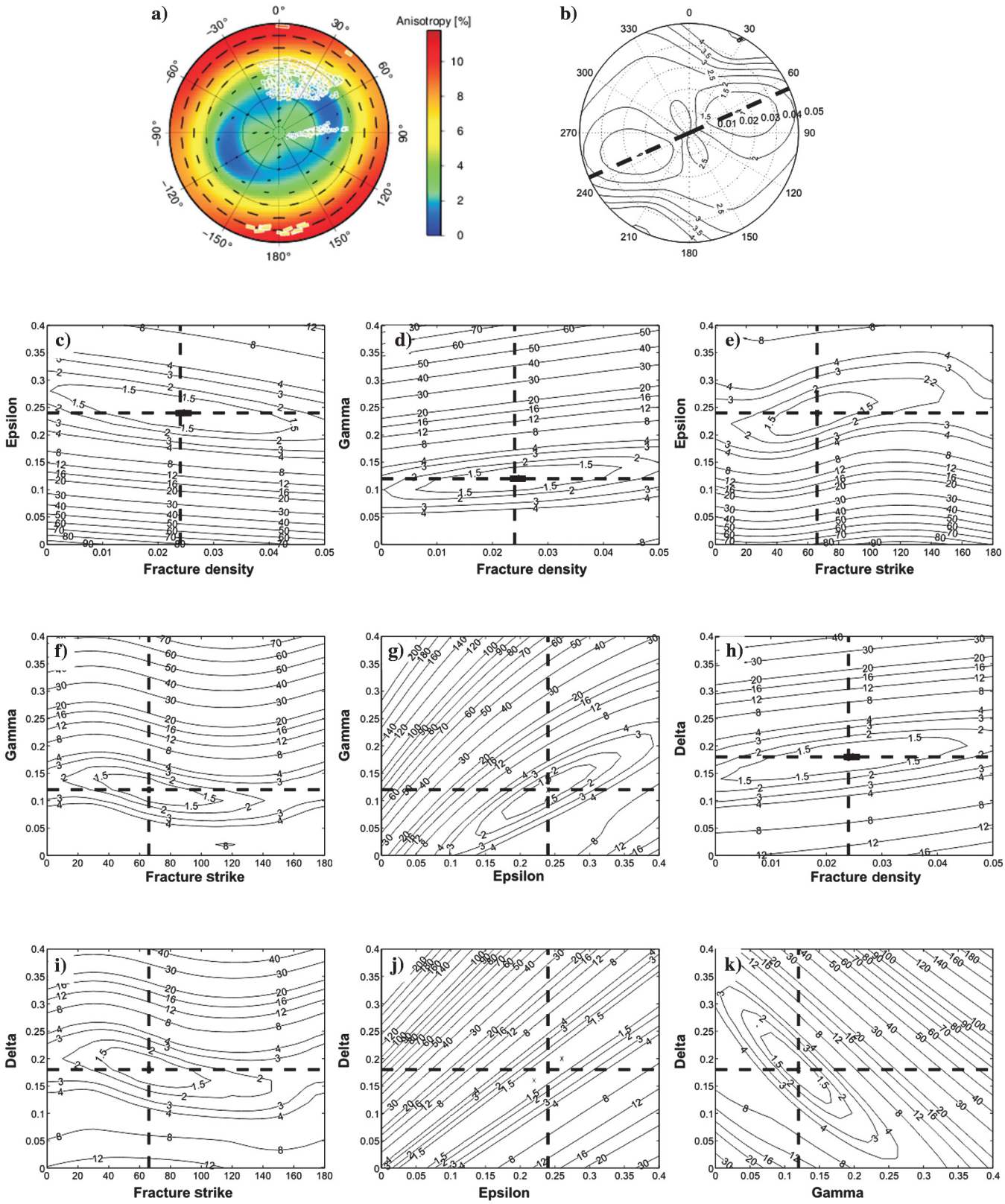

Figure 5. Inversion results for the entire data set, with ε, γ, δ, fracture density and fracture strike as free parameters. Panel (a) shows the splitting observations (white outlined ticks) overlain on the splitting predicted by the best fitting model (black ticks and contours). Panels (b–k) show slices through the misfit hypercube at the best fit values of the parameters not plotted, i.e., (c) shows misfit as a function of fracture density and ε at best fitting values of γ, δ, and fracture strike. In (b), fracture density is the radial coordinate, strike is polar angle. Other panels are as labeled.

as the fluid leaks off, causing the preexisting cracks in the surrounding medium to open or be more compliant, which in turn increases the anisotropy. This also occurs after pumping the main stage (near hour 15). Further, the anisotropy (i.e., fracture density) is minimum during the main and most sustained pumping stage. Note that detected seismic activity also trails the pumping pressure. We suggest that the fracture density does not remain at the higher level because the proppant does not reach these cracks to keep them open and fluid leaks off, which reduces the volume and thus stress on the rock.

DISCUSSION

We observe temporal variation in shear-wave-splitting delay time and our inversion of anisotropy parameters indicates a variable fracture density in the rock mass. We interpret that as crack opening and closure, whose seismic energy emission is too small to be detectable by the monitoring array. This cracking occurs within the rock mass in a region beyond the hydraulic fracture corridor, the latter being delineated by observed microseismic events. Three scenarios may explain the different orientation of cracks and the hydraulic fracture corridor (Figure 8). First, the fractures and cracks oriented at N66°E represent a joint set formed by a paleo (or regional) stress field with the maximum compressive horizontal stress orientation σ_H parallel to that direction. The current (or local) stress field is oriented parallel to the strike of the hydraulic fracture, which opens in a purely tensile mode. Nolen-Hoeksema and Ruff (2001) argue that overpressuring the rock by injection can result in such a deviation of the local stress field and leads to preferred fracture orientations deviating from the regional stress field. Second, the current and past stress field are oriented parallel to the (again tensionally opening) hydraulic fracture at N83°E and the fracture set at N66°E represents Riedel shears of a regional scale shearing process. The third alternative is a stress field σ_H parallel to the observed fracture orientation of N66°E. The hydraulic fracture corridor forms then as en-echelon failure (e.g., Pollard and Aydin, 1988) in a combination of tensile and shears fracturing oblique to the orientation of σ_H. If natural cracks and fissures exist already in the rock mass, they are likely to be reactivated due to a change in state of stress, even if they are not optimally oriented. These cracks join in an en-echelon fashion and form a larger scale hydraulic fracture, whose orientation deviates from the dominant crack strike (Figure 8).

The combination of shear and tensile failure in the Cotton Valley hydraulic fracture experiment has been inferred from moment tensor inversions. Generally, composite focal mechanisms determined by Rutledge et al. (2004) indicate both left- and right-lateral strike-slip faulting with slip planes subparallel to the strike of the hydraulic fracture. More recent full moment tensor inversions by Šílený et al. (2009) show evidence for a larger nondouble-couple component for events of the main fracture and more shear component for events of the off-strike cluster. In an earlier study, Urbancic et al. (1999) identified large b-values in the area of the cluster. Such observations have been related to multiple fractures along different orientations (Kagan, 1992), thus supporting the interpretation of complex and varied rupture mechanisms. In contrast to current models of a single fracture opening, it thus appears that complex rupture processes generate the fracture corridor. Such complex processes require full moment tensor inversions instead of double-couple focal mechanism analysis and may explain why our inferred dominant strike of cracks is oriented between the orientation of the composite focal mechanism of the reactivated fracture and that

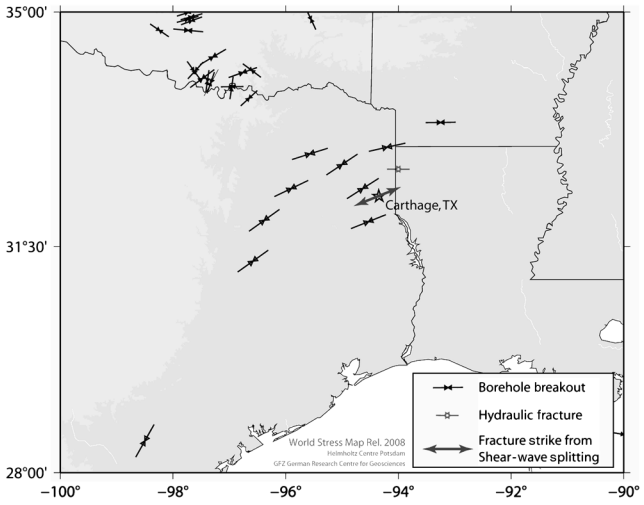

Figure 6. Regional stress orientations in the vicinity of the Carthage, Cotton Valley borehole from the World Stress Map (Heidbach et al., 2008). We note that these agree with the fracture orientation inferred from shear-wave splitting (which is N66E) and not with the main trend of the seismicity.

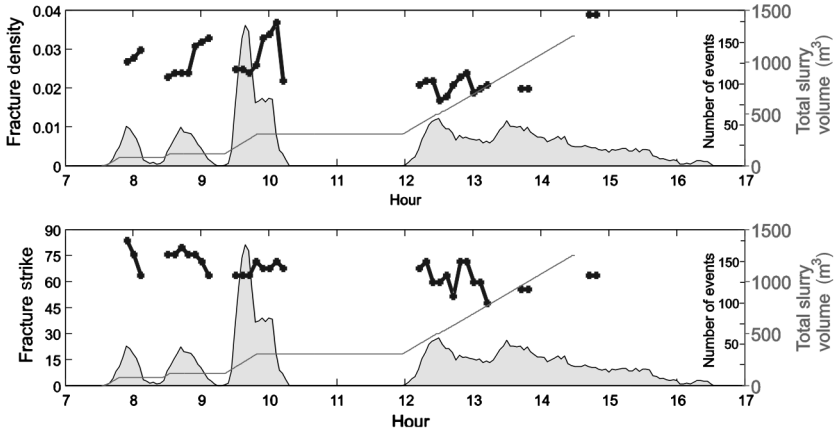

Figure 7. Temporal evolution of fracture density (top) and fracture strike (bottom) (both in blue). The cumulative slurry volume pumped into the formation is shown as green line. Also shown in gray filled area is the number of events occurring during each time window of the inversions.

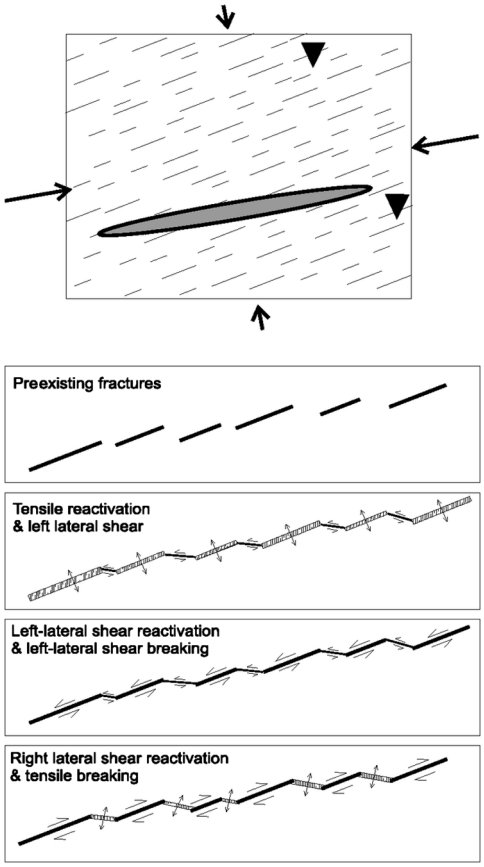

Figure 8. Model of Cotton Valley fracturing process. Top: joints and cracks form parallel to the regional stress field. The hydraulic fracture corridor opens at an angle to that orientation by a mixture of tensile and shears failure. Potential mechanisms for fracturing are outlined in the lower three panels.

of the main fracture (Figures 4 and 5 and Rutledge et al., 2004, respectively).

Our shear-wave-splitting analyses shows that the observed anisotropy can in part be attributed to preexisting cracks in the rock mass. Together with the observation by previous studies of shear and tensile components in moment tensors, our preferred interpretation for the Cotton Valley hydraulic fracture experiment is that shear and tensile failure connects preexisting joints and fissures, forming a fracture corridor oblique to the regional stress direction (Figure 8).

CONCLUSION

Shear-wave-splitting analysis of microseismic events from the Cotton Valley hydraulic fracture experiment shows that microseismic events can be used for reservoir characterization well beyond the source regions. Inversion of the shear-wave-splitting data reveals a nonzero Thomsen's γ parameter, implying anisotropy due to the sedimentary fabric, which is in agreement with observations from previous in laboratory studies. The inversion also indicates a dominant fracture orientation of N66°E within the reservoir, in agreement with regional borehole breakout measurements, but oblique to the induced hydraulic fracture trend. We attribute this to a series of en-echelon ruptures, which connect preexisting joints and cracks.

Our shear-wave-splitting results show an increase in anisotropy within a localized cluster of events, and we conclude that only a temporal increase in the activation of fissures and cracks (at subseismic detection levels) can cause the observed change in anisotropy. The activation must, however, occur within an elliptical halo around the main fracture. The halo radius is estimated to be between 85 and 127.5 m and may well account for a large amount of fluid loss. The fracturing of rock beyond the fracture corridor has wide implications for the effective permeability and thus efficiency of a hydraulic fracture treatment.

We have shown that shear-wave-splitting analysis broadens the utility of microseismic data that are routinely acquired during hydraulic stimulations. It provides a means of monitoring the extent, orientation, and magnitude of hydraulic fracture stimulation beyond the actual event locations. A temporal variation of fracturing in the rock matrix correlates well with pumping stages and the accompanying seismicity. The observation that fracture density returns to background level after each cycle implies that in this experiment, the connectivity of the cracks with the main fracture is small and proppant does not penetrate very far into the surrounding rock. The overall decrease in inverted fracture density can be attributed to crack closure due to compressive stresses following the fluid injection. This suggests that shear-wave-splitting analysis could provide a very useful tool to monitor the extent of the subseismically stimulated reservoir volume and the placement of proppant into a hydraulic fracture.

ACKNOWLEDGMENTS

We thank the editor, Vladimir Grechka, the associate editor, Shawn Maxwell, and three reviewers for constructive comments that have improved the manuscript. Funding for the work has been provided by the sponsors of the Bristol University Microseismicity Projects (BUMPS).

APPENDIX A

STABILITY OF INVERSION

To assess the ability of the inversion procedure to accurately identify fracture strike and density, we present an analysis of error using synthetic data. The parameters controlling the elastic stiffness tensor, from which we forward model shear-wave splitting to be compared with observation, are the background P- and S-wave velocities (V_P, V_S), fracture strike (α), fracture density (ξ), and Thomsen's parameters ε, γ, and δ. The free parameters we use in our inversion are α, ξ, γ, and δ. Therefore, erroneous choices of ε, V_P, and V_S, which must be fixed in the inversion, have the potential to influence the inversion results. We constrain V_P and V_S based on the velocity model used to compute event locations. Thomsen's ε parameter may be estimated using controlled source seismic data or laboratory core measurements, but for our purposes may be considered to be unconstrained. The purpose of this error analysis is to estimate whether fixing ε, V_P and V_S using erroneous values impedes us in constraining fracture parameters.

We generated an initial elastic model using as input parameters: fracture strike = N70°E, $\xi = 0.04$, $\varepsilon = 0.24$, $\gamma = 0.12$, $\delta = 0.06$, $V_P = 5000$ ms^{-1}, $V_S = 3000$ ms^{-1}. This model was illuminated using a randomly selected subset of 150 of the 1500 Cotton Valley observations, and the resulting shear-wave splitting was modeled. We add noise to the synthetically generated data set, using a

uniform distribution within $\pm 10°$ for arrival azimuth and inclination, $\pm 10°$ to the fast shear-wave polarization direction, and $\pm 0.5\%$ to the percentage velocity difference between fast and slow shear waves. These noisy data were then inverted using erroneous values for ε, V_P, and V_S, randomly selected from a uniform distribution within $V_{(P,S)} = V \pm (V \times 10\%)$, $\varepsilon = \varepsilon \pm (\varepsilon \times 100\%)$. The inversions using incorrect ε, V_P, and V_S was repeated 100 times. The ability (or failure) of the inversion to recover the initial model parameters, despite erroneous choices for ε, V_P, and V_S, will show how well-constrained we might consider our results to be.

The results of this error analysis are shown in Figure A-1. The lower three panels show the erroneously fixed values of ε, V_P, and V_S. The upper four panels show histograms of the free parameters recovered by the inversion. The standard deviations of the recovered distributions are also given. We note that strike, ξ and γ appear to be well-constrained, while δ is unconstrained. The inaccuracies in δ can be understood by considering Figure 5j, where it is apparent that δ and ε trade-off against each other. Therefore, an inaccurate choice of fixed ε must cause an inaccurate value of δ to be recovered. Laboratory measurements or controlled source seismic data may help to constrain ε, permitting accurate recovery of δ. However, as no such data is available here, δ is unconstrained. Importantly, however, Figure A-1 shows that the lack of constraint in δ does not contaminate our estimates of α and ξ. The results presented in Figure A-1 should inform our analysis presented above, showing the extent to which the parameters can be constrained.

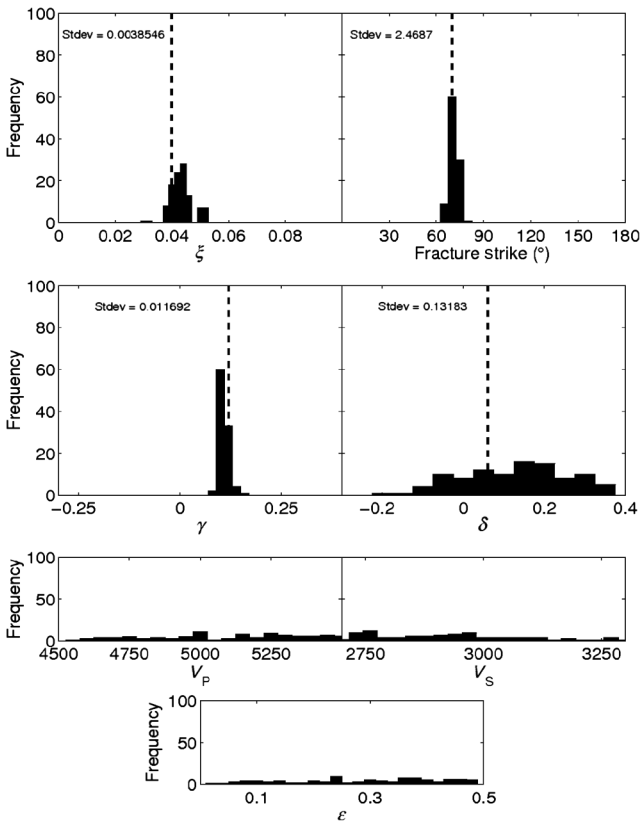

Figure A-1. Error analysis results. The upper four plots show histograms of the values recovered by the inversion, using the erroneous values of ε, V_P and V_S shown in the lower three panels. The dashed lines show the parameters used to generate the initial model. Fracture density and strike, and γ, are well recovered, while δ is unconstrained.

REFERENCES

Ake, J., K. Mahrer, D. O'Connell, and L. Block, 2005, Deep-injection and closely monitored induced seismicity at Paradox Valley, Colorado: Bulletin of the Seismological Society of America, **95**, 664–683, doi: 10.1785/0120040072.

Al-Harrasi, O., A. Al-Anboori, A. Wüstefeld, and J.-M. Kendall, 2011a, Seismic anisotropy in a hydrocarbon field estimated from microseismic data: Geophysical Prospecting, **59**, 227–243, doi: 10.1111/gpr.2011.59.issue-2.

Al-Harrasi, O., J.-M. Kendall, and M. Chapman, 2011b, Fracture characterisation using frequency — Dependent shear wave anisotropy analysis of microseismic data: Geophysical Journal International, **185**, 1059–1070, doi: 10.1111/gji.2011.185.issue-2.

Angus, D. A., J-M. Kendall, Q. J. Fisher, J. M. Segura, S. Skachkov, A. J. L. Crook, and M. Dutko, 2010, Modelling microseismicity of a producing reservoir from coupled fluid — Flow and geomechanical simulation: Geophysical Prospecting, **58**, 901–914, doi: 10.1111/j.1365-2478.2010.00913.x.

Backus, G. E., 1964, Geographical interpretation of measurements of average phase velocities of surface waves over great circular and great semi-circular paths: Bulletin of the Siesmological Society of America, **54**, no. 2, 571–610.

Bakulin, A., V. Grechka, and I. Tsvankin, 2000, Estimation of fracture parameters from reflection seismic data — Part II: Fractured models with orthorhombic symmetry: Geophysics, **65**, 1803–1817, doi: 10.1190/1.1444864.

Crampin, S., 1984, Effective anisotropic elastic constants for wave propagation through cracked solids: Geophysical Journal of the Royal Astronomical Society, **76**, 135–145, doi: 10.1111/j.1365-246X.1984.tb05029.x.

Foulger, G. R., B. R. Julian, D. P. Hill, A. M. Pitt, P. E. Malin, and E. Shalev, 2004, Non-double-couple microearthquakes at Long Valley Caldera, California, provide evidence for hydraulic fracturing: Journal of Volcanology and Geothermal Research, **132**, no. 1, 45–71, doi: 10.1016/S0377-0273(03)00420-7.

Gerst, A., and M. K. Savage, 2004, Seismic anisotropy beneath Ruapehu volcano: A possible eruption forecasting tool: Science, **306**, 1543–1547, doi: 10.1126/science.1103445.

Grechka, V., S. Theophanis, and I. Tsvankin, 1999, Joint inversion of P- and PS-waves in orthorhombic media: Theory and a physical-modeling study: Geophysics, **64**, 146–161, doi: 10.1190/1.1444512.

Hall, S. A., and J-M. Kendall, 2003, Fracture characterisation at Valhall: Application of P-wave AVOA analysis to a 3D ocean-bottom data set: Geophysics, **68**, 1150–1160, doi: 10.1190/1.1598107.

Hall, S. A., J-M. Kendall, J. Maddock, and Q. Fisher, 2008, Crack density tensor inversion for analysis of changes in rock frame architecture: Geophysical Journal International, **173**, 577–592, doi: 10.1111/gji.2008.173.issue-2.

Heidbach, O., M. Tingay, A. Barth, J. Reinecker, D. Kurfeß, and B. Müller, 2008, The World Stress Map database release 2008, doi: 10.1594/GFZ.WSM.Rel2008.

Jones, J. R., and L. K. Britt, 2009, Design and appraisal of hydraulic fractures: Society of Petroleum Engineers Journal, 150.

Kachanov, M., 1980, Continuum model of medium with cracks: Journal of the Engineering Mechanics Division, American Society of Civil Engineers, **106**, 1039–1051.

Kagan, Y. Y., 1992, On the geometry of an earthquake fault system: Physics of the Earth and Planetary Interiors, **71**, 15–35, doi: 10.1016/0031-9201(92)90025-Q.

Keir, D., J-M. Kendall, C. J. Ebinger, and G. W. Stuart, 2005, Variations in late syn-rift melt alignment inferred from shear wave splitting in crustal earthquakes beneath the Ethiopian rift: Geophysical Research Letters, **32**, L23308, doi: 10.1029/2005GL024150.

Kendall, J.-M., G. W. Stuart, C. J. Ebinger, I. D. Bastow, and D. Keir, 2005, Magma-assisted rifting in Ethiopia: Nature (London), **433**, no. 7022, 146–148, doi: 10.1038/nature03161.

Laubach, S. E., 1988, Subsurface fractures and their relationship to stress history in east Texas sandstone: Tectonophysics, **156**, 37–49, doi: 10.1016/0040-1951(88)90281-8.

Nolen-Hoeksema, R. C., and L. J. Ruff, 2001, Moment tensor inversion of microseisms from the B-sand propped hydrofracture, M-site, Colorado: Tectonophysics, **336**, 163–181, doi: 10.1016/S0040-1951(01)00100-7.

Pollard, D. D., and A. Aydin, 1988, Progress in understanding jointing over the past century: GSA Bulletin, **100**, 1181–1204, doi: 10.1130/0016-7606(1988)100<1181:PIUJOT>2.3.CO;2.

Raymer, D. G., A. Tommasi, and J-M. Kendall, 2000, Predicting the seismic implications of salt anisotropy using numerical simulations of halite deformation: Geophysics, **65**, 1272–1280, doi: 10.1190/1.1444818.

Rozhko, A. Y., 2010, Role of seepage forces on seismicity triggering: Journal of Geophysical Research, **115**, B11314, doi: 10.1029/2009JB007182.

Rutledge, J. T., and W. S. Phillips, 2003, Hydraulic stimulation of natural fractures as revealed by induced microearthquakes, Carthage Cotton Valley gas field, east Texas: Geophysics, **68**, 441-452, doi: 10.1190/1.1567212.

Rutledge, J. T., W. S. Phillips, and M. J. Mayerhofer, 2004, Faulting induced by forced fluid injection and fluid flow forced by faulting: An interpretation of hydraulic-fracture microseismicity, Carthage Cotton Valley Gas Field, Texas: Bulletin of the Seismological Society of America, **94**, 1817–1830, doi: 10.1785/012003257.

Schoenball, M., T. M. Müller, B. I. R. Müller, and O. Heidbach, 2010, Fluid-induced microseismicity in pre-stressed rock masses: Geophysical Journal International, **180**, 813–819, doi: 10.1111/gji.2010.180.issue-2.

Šílený, J., D. P. Hill, L. Eisner, and F. H. Cornet, 2009, Non-double-couple mechanisms of microearthquakes induced by hydraulic fracturing: Journal of Geophysical Research, **114**, B08307, doi: 10.1029/2008JB005987.

Silver, P. G., and W. W. Chan, 1991, Shear wave splitting and subcontinental mantle deformation: Journal of Geophysical Research, **96**, 16429–16454, doi: 10.1029/91JB00899.

Strubhar, M. K., J. L. Fitch, and E. E. Glenn, 1975, Multiple vertical fractures from an inclined wellbore — A field experiment: Journal of Petroleum Technology, **27**, 641–647, doi: 10.2118/5115-PA.

Teanby, N. A., J.-M. Kendall, and M. van der Baan, 2004, Automation of shear wave splitting measurements using cluster analysis: Bulletin of the Seismological Society of America, **94**, 453–463, doi: 10.1785/0120030123.

Thomsen, L., 1986, Weak elastic anisotropy: Geophysics, **51**, 1954–1966, doi: 10.1190/1.1442051.

Tsvankin, I., 1997, Moveout analysis in transversely isotropic media with a tilted symmetry axis: Geophysical Prospecting, **45**, 479–512, doi: 10.1046/j.1365-2478.1997.380278.x.

Urbancic, T. I., V. Shumila, J. T. Rutledge, and R. J. Zinno, 1999, Determining hydraulic fracture behavior using microseismicity: Paper presented at the meeting of the Vail Rocks 99, 37th US Rock Mechanics Symposium.

Valcke, S. L. A., M. Casey, G. E. Lloyd, J-M. Kendall, and Q. J. Fisher, 2006, Lattice preferred orientation and seismic anisotropy in sedimentary rocks: Geophysical Journal International, **166**, 652–666, doi: 10.1111/gji.2006.166.issue-2.

Verdon, J. P., D. A. Angus, J-M. Kendall, and S. A. Hall, 2008, The effect of microstructure and nonlinear stress on anisotropic seismic velocities: Geophysics, **73**, no. 4, D41–D51, doi: 10.1190/1.2931680.

Verdon, J. P., and J.-M. Kendall, 2011, Detection of multiple fracture sets using observations of shear-wave splitting in microseismic data: Geophysical Prospecting, **59**, 593–608, doi: 10.1111/gpr.2011.59.issue-4.

Verdon, J., J.-M. Kendall, and A. Wuestefeld, 2009, Imaging fractures and sedimentary fabrics using shear wave splitting measurements made on passive seismic data: Geophysical Journal International, **179**, 1245–1254, doi: 10.1111/gji.2009.179.issue-2.

Walker, R. N., 1997, Cotton Valley hydraulic fracture imaging project: Paper presented at the meeting of the SPE Annual Technical Conference and Exhibition.

Wuestefeld, A., O. Al-Harrasi, J. P. Verdon, J. Wookey, and J. M. Kendall, 2010, A strategy for automated analysis of passive microseismic data to image seismic anisotropy and fracture characteristics: Geophysical Prospecting, **58**, 755–773, doi: 10.1111/j.1365-2478.2010.00891.x.

Wuestefeld, A., and G. H. R. Bokelmann, 2007, Null detection in shear wave splitting measurements: Journal of Geophysical Research, **97**, 1204–1211, doi: 10.1785/0120060190.

Wuestefeld, A., G. H. R. Bokelmann, C. Zaroli, and G. Barruol, 2008, SplitLab: A shear wave splitting environment in Matlab: Computers & Geosciences, **34**, 515–528, doi: 10.1016/j.cageo.2007.08.002.

Wuestefeld, A., J. M. Kendall, J. P. Verdon, and A. van As, 2011, In situ monitoring of rock fracturing using shear wave splitting analysis: An example from a mining setting: Geophysical Journal International, **187**, no. 2, 848–860, doi: 10.1111/gji.2011.187.issue-2.

Zatsepin, S. V., and S. Crampin, 1997, Modelling the compliance of crustal rock — I. Response of shear-wave splitting to differential stress: Geophysical Journal International, **129**, 477–494, doi: 10.1111/gji.1997.129.issue-3.